Applied Food Research 6 (2026) 102013

Contents lists available at ScienceDirect

Applied Food Research

journal homepage: www.elsevier.com/locate/afres

Optimization of print fidelity, efficiency and texture of 3D printed gluten-free snacks using artificial neural network-genetic algorithm modeling

Lidija Perović [a], Jovana Simeunović [a], Jelena Jovančević [b], Jelena Miljanić [a], Bojana Kokić [a], Slobodan Birgermajer [b], Predrag Kojić [c], Jovana Kojić [b,*]

[a] Institute of Food Technology in Novi Sad, University of Novi Sad, Bulevar Cara Lazara 1, 21000 Novi Sad, Serbia
[b] BioSense Institute - Research and Development Institute for Information Technologies in Biosystems, University of Novi Sad, Dr Zorana Đinđića 1a, 21000 Novi Sad, Serbia
[c] Faculty of Technology Novi Sad, University of Novi Sad, Bulevar cara Lazara 1, 21000 Novi Sad, Serbia

ARTICLE INFO

Keywords:
3D food printing
Gluten-free 3D snack
Print fidelity
Texture optimization
ANN-GA modelling

ABSTRACT

3D food printing (3DFP) is emerging as a transformative technology for producing customized, nutritionally tailored foods, with growing potential for commercial applications in the health-oriented and gluten-free markets. In this study, gluten-free 3D-printed snacks were developed from proso millet flour, almond protein, and yeast protein, and the influence of infill percentage (I), extrusion multiplier (EM), printing speed (PS), and layer height (LH) on dimensional fidelity, texture, and process efficiency was systematically evaluated. EM was the dominant driver of dimensional accuracy ($r \approx 0.80$ for both length and width), reflecting its critical role in controlling material flow and deposition precision. Post-processing preserved shape accuracy, although limited height variation occurred due to vapor-induced puffing. Denser structures exhibited lower baking loss (31.17–43.77 %), confirming density as the key determinant of moisture release. Hardness (3.38–38.62 N) was predicted with high accuracy using an artificial neural network–genetic algorithm (ANN–GA) model (R^2 = 0.968–0.981, RMSE = 1.271–1.903). A precise interplay between EM, I, PS, and LH was identified as essential for simultaneously optimizing dimensional stability, textural quality, and process efficiency. Sensitivity analysis identified EM (60.89 %) and I (27.18 %) as key positive contributors to textural quality, whereas LH (–8.86 %) and PS (–3.08 %) had negative impacts. ANN–GA optimization reduced printing time by 33 % (to 3 min) while maintaining product quality (CQ = 4.67), demonstrating an effective tool for balancing speed, fidelity, and structural stability.

1. Introduction

Pressing global challenges such as climate change, natural resource reduction, and hunger are intensified by the rapid population growth, which is projected to reach 9.7 billion by 2050 (FAO, 2018). Additionally, hectic lifestyles and increased awareness of the importance of healthy eating have driven demand for novel, non-conventional, and healthier alternatives for their daily diet (Maldonado-Rosas et al., 2022). In this context, three-dimensional food printing (3DFP) has emerged as a promising technology, enabling layer-by-layer fabrication of customized, nutritionally tailored, and geometrically complex food structures (Agarwal et al., 2022; Guénard-Lampron et al., 2023; Derossi et al., 2023). Recent studies have demonstrated the versatility of 3DFP with a wide range of food matrices, including chocolate (Dordević et al., 2025), gels (Shi et al., 2024), plant-based meat analogues (Cheng et al., 2024), fruit and vegetable by-streams (Tyupova & Harasym, 2024), and various pseudo-cereals and cereals (Agarwal et al., 2022; Radoš et al., 2023a, 2023b; Mustač et al., 2023; Pradhan et al., 2025).

Among gluten-free grains, proso millet (*Panicum miliaceum L*) holds significant potential to contribute to a more resilient and sustainable future, fostering several Sustainable Development Goals (SDGs) of the UN, which makes a compelling case for its integration into global food systems (Derossi et al., 2023). However, despite its advantages, gluten-free doughs present challenges in 3DFP in terms of elasticity,

* Corresponding author.
E-mail address: jovana.kojic@biosense.rs (J. Kojić).

https://doi.org/10.1016/j.afres.2026.102013
Received 26 January 2026; Received in revised form 2 April 2026; Accepted 13 April 2026
Available online 14 April 2026
2772-5022/© 2026 The Authors. Published by Elsevier B.V. This is an open access article under the CC BY license (http://creativecommons.org/licenses/by/4.0/).

shape stability and structural integrity (Pradhan et al., 2025). To address these challenges, plant-based protein materials, often rich in fiber, can be incorporated into formulations to improve not only the nutritional profile but also rheological behaviour, extrusion performance, and mechanical stability of the dough (Jiang et al., 2019). In our previous work (Simeunović et al., 2025), a millet-based gluten-free formulation enriched with almond and yeast proteins was successfully developed, with the primary aim of optimizing dough composition to improve nutritional value, printability, and sensory attributes of the resulting snacks. However, since the incorporation of protein-based materials naturally affects dough flow and extrusion, careful adjustment of printing parameters is essential to maintain shape fidelity and structural integrity.

Printability, a key factor in 3DFP, reflects a material's capacity to flow smoothly, retain its shape, and maintain dimensional stability throughout and after extrusion (Kadival et al., 2023). This property depends on both the material's characteristics and process parameters, ensuring stable layer formation and structural integrity post-printing. Print quality refers to the overall accuracy, consistency, and visual integrity of a 3D printed object in relation to its intended design. It is influenced by factors such as extrusion behaviour, dimensional fidelity and shape stability (Mustač et al., 2023). Among the numerous factors affecting printability, infill percentage (Huang et al., 2019), extrusion rate (Pradhan et al., 2025), printing speed (Arora & Prithviraj, 2022), and layer height (Severini et al., 2016) play dominant roles by influencing extrusion flow, layer adhesion, dimensional fidelity, and overall product quality. In particular, maintaining height fidelity is often the most challenging due to gravitational effects and layer compaction during printing (Mallesham et al., 2024). In addition to structural quality, long printing time remains one of the major bottlenecks limiting the scalability of 3DFP toward semi-industrial production (Oropallo & Piegl, 2016; Rogers & Srivastava, 2021), highlighting the need for process optimization strategies that simultaneously address quality and efficiency.

Despite the growing interest in 3D food printing, direct comparisons with conventional manufacturing techniques such as molding remain relatively limited. Previous studies have shown that the manufacturing approach itself can significantly influence the structure and quality attributes of bakery products. For instance, extrusion-based 3D printing can modify the internal cellular structure, resulting in differences in cell diameter, wall thickness, and porosity compared with traditionally molded dough systems (Kewuyemi et al., 2022). Importantly, parameters such as infill percentage and extrusion multiplier are specific to additive manufacturing and cannot be directly reproduced using conventional molding. Unlike molded products, where the internal structure is generally homogeneous, 3D printing enables precise control of internal architecture through adjustable infill parameters, allowing targeted modification of porosity, density, and mechanical properties (Montero et al., 2025; Sun et al., 2015).

Traditionally, optimization has been performed using response surface methodology (RSM), a statistical multivariate technique suitable for modeling linear and moderately nonlinear relationships (Chelladurai et al., 2021). However, since RSM relies on second-order polynomial functions, its ability to capture highly nonlinear behaviors and manage multidimensional datasets is inherently constrained, often reducing predictive reliability (Baş et al., 2007). Consequently, the implementation of artificial intelligence (AI) techniques has emerged as a powerful alternative, offering enhanced flexibility and accuracy in process optimization. AI-based models can adaptively learn from complex experimental data and improve predictive performance over time. Within this framework, various machine learning (ML) algorithms, such as support vector machines, random forests, and particularly artificial neural networks (ANNs), have been successfully applied across food and materials engineering domains (Moon et al., 2022) thanks to their strong capacity to model nonlinear, multidimensional relationships and generalize effectively to unseen data (Jiao et al., 2024; Bao et al., 2024; Carvajal-Mena et al., 2023; Wang et al., 2023).

Nevertheless, most prior applications of machine learning in 3D food printing (3DFP) have primarily focused on predictive modelling and have rarely been integrated with optimisation algorithms to derive optimal process parameters. Artificial neural networks (ANNs) are commonly employed to establish nonlinear mappings between printing parameters and quality-related responses; however, when used alone they primarily provide predictions and do not inherently offer a mechanism for identifying optimal parameter combinations under competing performance criteria. Improvements in one response frequently lead to deterioration in another, introducing multi-objective trade-offs that cannot be effectively resolved through prediction-only modelling approaches (Bao et al., 2024; Jiao et al., 2024; Habuš et al., 2022). Consequently, both ANN-based predictive modelling and conventional statistical approaches such as response surface methodology (RSM) remain limited in their ability to derive robust operational parameter recommendations for complex printing systems (Lee & Hashimoto, 2024). To address this gap, the present study integrates ANN modelling with a genetic algorithm (ANN–GA), enabling simultaneous optimisation of multiple responses and systematic identification of parameter combinations that balance printing efficiency and product quality.

Following our previous work (Simeunović et al., 2025), which developed a gluten-free formulation, the present study focuses on the optimization of printing parameters. The aim is to apply a hybrid artificial neural network–genetic algorithm (ANN–GA) framework to investigate the combined effects of infill percentage (I), extrusion multiplier (EM), printing speed (PS), and layer height (LH) on the print quality, shape fidelity, and texture characteristics of gluten-free millet-based snacks enriched with almond and yeast proteins. The proposed ANN–GA framework identifies optimal printing conditions that maximize dimensional stability, improve mechanical integrity, and reduce overall printing time. Furthermore, coupling ANN with a genetic algorithm enables efficient exploration of complex nonlinear parameter interactions, facilitating the identification of robust parameter combinations and providing a data-driven framework for future optimisation of 3D food printing processes.

2. Materials and methods

2.1. Materials

Saccharomyces cerevisiae (yeast) protein cookie flavour (75.87 % proteins, 9.14 % fat, 6.40 % dietary fibers, 4.52 % moisture) under the commercial name Smartein was kindly donated by Pharma Intelligence, Novi Sad, Serbia. The proso millet flour (10.15 % proteins, 2.96 % fat, 3.90 % dietary fibers, 9.36 % moisture) (Interpak, Kraljevo, Serbia), almond protein (46.2 % proteins, 15.5 % fat, 5.11 % moisture) (Crazy nutrition, Belgrade, Serbia), almond butter with cinnamon (20.18 % proteins, 48.89 % fat) (Granum, Hajdukovo, Serbia) were purchased from the local supermarket in Novi Sad, Serbia.

2.2. Methods

2.2.1. Ink preparation

Ingredients were not subjected to any thermal or mechanical pretreatment prior to ink preparation. The optimized ink formulation was prepared using 32 % of proso millet flour, 8 % of yeast protein (YP), and 8 % of almond protein, following the formulation strategy previously reported by Simeunović et al. (2025). A 0.5-mm sieve was used for all fractions to ensure consistency in the particle size range. Almond butter with cinnamon (11 %) was tempered at room temperature (25 °C) and added to the dry ingredients. The mixture was initially mixed manually with a spatula in a circular motion. Afterwards, the tap water (41 %) was added, and the mixture was homogenized for 1 min on 300 rpm using a hand mixer (MX2002, VOX, Serbia) to form cohesive dough and left to rest for 30 min at room temperature covered with a cloth. All

experiments were conducted in an ISO 17025-accredited laboratory under controlled environmental conditions ensuring reproducibility and accuracy of all measurements. Temperature and relative humidity were continuously monitored to ensure stable environmental conditions and minimize potential variability in water migration and rheological behavior of the dough.

2.2.2. Design of experiment

The overall experimental workflow, including dough preparation, design of experiments, 3D printing, post-processing, quality evaluation, and ANN–GA modeling, is schematically presented in Fig. 1.

A four factor (k), five level (L) central composite design (CCD), with seven centre points (C0) was applied to establish the experimental framework for 3D printing variables using statistical software (Minitab, Pennsylvania, USA). A total of 31 experimental runs were performed, comprising 16 factorial points (full 24 design), 8 axial points ($\alpha = 1.682$), and 7 centre point replicates (Run 6, 7, 9, 19, 25, 28, 31), enabling systematic investigation of 3D printing parameters while maintaining relatability of the design space. All experiments were conducted five times, with each replicate representing a separate 3D-printed shape prepared from the same dough batch and all following measurements were performed on these individual shapes. These technical replicates reflect the reproducibility of the printing and measurement process.

The input parameters investigated in this work were infill percentage (I), extrusion multiplier (EM), print speed (PS), and layer height (LH). The layer height was defined as a percentage share of the nozzle diameter. The specific parameter values were selected based on preliminary experiments and literature recommendations (Derossi et al., 2018; Arora & Prithviraj, 2022; Bulut & Candoğan, 2022; Kim et al., 2024), while all other printing parameters were kept constant to clearly isolate the effects of the investigated parameters and guarantee the reliability of experimental outcomes. Table 1 represents the actual and coded values of the independent factors.

Table 1
3D printing parameters and levels of experimental design.

3D printing parameters	Symbol	Level				
		-1.682	-1	0	1	1.682
Infill percentage (%)	I	10	30	50	70	90
Extrusion multiplier (%)	EM	30	60	90	120	150
Print speed (mm/s)	PS	5	10	15	20	25
Layer height (%)	LH	10	30	50	70	90

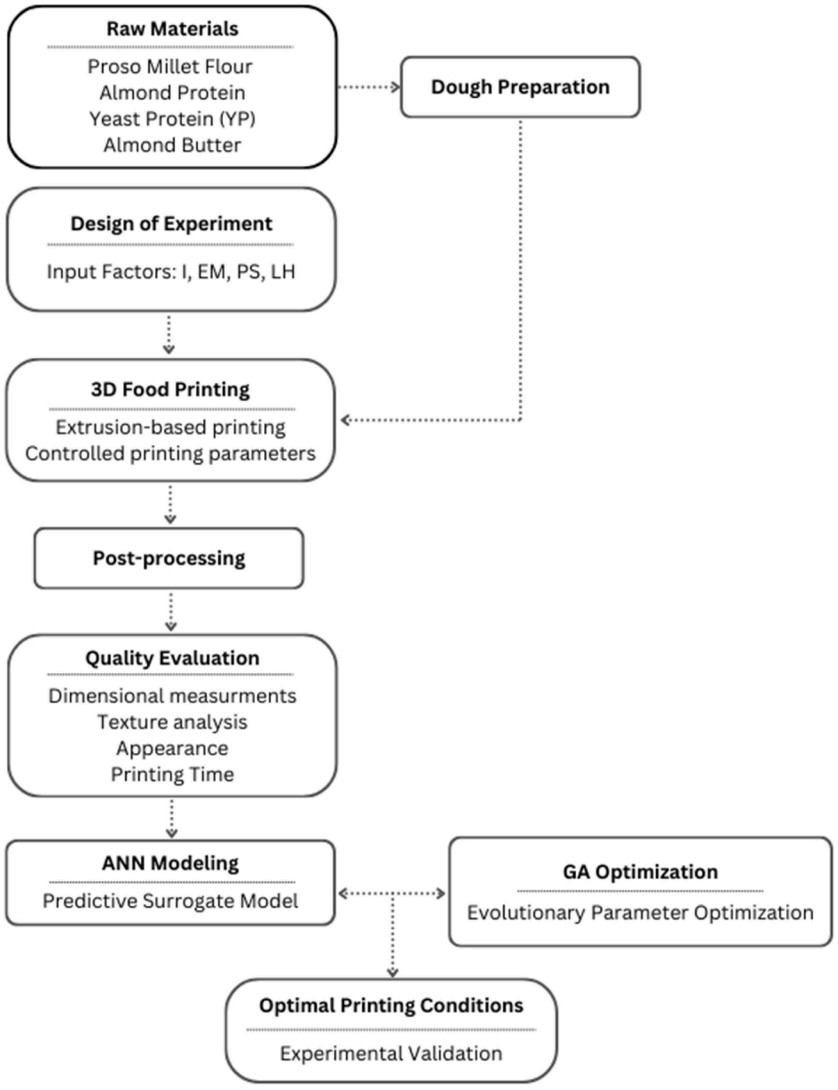

Fig. 1. Schematic overview of the experimental workflow, including dough preparation, design of experiments, 3D printing, post-processing, quality evaluation, and ANN–GA modeling.

2.2.3. 3D printing process

Five samples of each probe were printed using a 3D Food printer (Felix Food 1.5, Felix printers, Netherlands) into a butterfly shape (dimensions: 60 mm x 60 mm x 6 mm). Computer-aided design (CAD) of a butterfly was designed on Autodesk 3ds Max 2022.2 (Autodesk Incorporation, San Francisco, CA, USA). The butterfly shape was saved as a stereolithography (STL) extension file. The Simplify3D software version 5.1.2 enables slicing of the 3D model layer by layer prior to printing. The extrusion system of the 3D printer is constructed of syringe (100 ml capacity) with retractable plunger and stainless-steel nozzle with internal diameter 1.6 mm (14 G). The syringe filled with dough was preheated to 35 °C before the start of the print. Grid infill pattern was selected for all samples.

2.2.4. Post-processing

Post-processing of the printed 3D samples was performed using a drying oven with air flow (Sterimatic ST-11, Instrumentaria, Zagreb, Croatia), at 150 °C until constant mass of the 3D snacks. Mass of the raw and baked snack was measured on technical balance (BWL 61, Boeco, Germany). The oven was pre-heated at 150±1 °C for 1 h. Each sample was baked individually, placing the 3D-printed snacks at the center of the oven. The end time for baking was determined during preliminary research individually for each run according to time required to reach constant moisture within the snack below 5 % (Radoš et al., 2023a; Liu & Zhang, 2021). Moisture content was measured using a moisture analyzer (model HE53, Mettler Tolledo, USA) for fast checking of moisture content. Additionally, baking loss was calculated using following equation (Pulatsu et al., 2020):

$$Baking\ loss\ (\%) = \frac{m_0 - m_1}{m_0} * 100 \quad (1)$$

where m_0 is the weight of a 3D snack after printing and m_1 is the weight after post-processing.

2.2.5. Print and product quality

The printed samples were scanned using an optical 3D scanner (Transcan C, Shinning 3D, China) equipped with EXScan C software version 1.4.2.1 in order for printing quality examination. The geometrical measurements of 3D snack samples were conducted in Siemens Solid Edge 2022 software version 222.00.00132. Print quality refers to evaluation of dimensions of a 3D sample: length (L), height (H) and width (W). The target measurements (length (L) = 60 mm, width (W) = 60 mm and height (H) = 6 mm) were determined from the CAD 3D model (Fig. 2). Responses such as shape fidelity and deformation were calculated using measurements, both, after printing and after post-processing. The 3D snack after printing was frozen at -20 °C for 30 min before the scanning to keep the snack shape unchanged. After baking, the samples were left at room temperature for 3 hours prior to physical analysis.

Shape fidelity refers to the ability of the printing ink to retain its intended shape upon deposition and it is typically assessed by comparing the actual dimensions of the printed samples to the theoretical dimensions defined by the CAD model (Mustač et al., 2023). The target value for shape fidelity is 100 %. Shape fidelity of 3D snacks after printing was calculated according to equation:

$$Shape\ fidelity\ (\%) = \frac{X_1}{X_0} \times 100, \quad (2)$$

where X_0 is the dimension of the 3D CAD model projected in Simplify3D software and X_1 is the dimension of the 3D snack after printing.

The effect of post-processing on the shape of 3D-printed snacks was determined as a percentile deviation of dimensions before and after baking, using following equation (Pulatsu et al., 2020):

$$Deformation\ (\%) = \frac{X_0 - X_1}{X_0} \times 100, \quad (3)$$

where X_0 is the dimension of the 3D snack after printing and X_1 is the dimension of 3D snack after baking.

Lastly, each sample received a print score from 1 (print failed) to 5 (excellent quality) based on visual inspection, following Radoš et al. (2023b), with adaptations for the current study.

The overall print quality, referred to as the composite quality score (CQ), was calculated as the arithmetic mean of the visual score (print score) and the dimensional fidelity score (fidelity score), thereby integrating both geometric accuracy and observable extrusion performance into a single quantitative metric. Equal weighting was adopted to ensure proportional contribution of visual layer integrity and dimensional stability to the overall assessment of structural print quality. The visual score reflects observable printing characteristics such as layer adhesion, surface continuity, and resistance to deformation, while the dimensional fidelity score represents the average geometric accuracy across three key dimensions: length, width, and height.

For each dimension, the fidelity score was calculated using the following formula:

$$fidelity_{dim} = 5 - 3 \times \frac{(dim - 100)^2}{(global_max_diff)^2} \quad (4)$$

where dim is the percentage accuracy of the given dimension (length, width, or height). The term global_max_diff is defined as the maximum absolute deviation from 100 % across all samples and all target dimensions, computed as:

$$global_max_diff = max(|dim - 100|) \quad (5)$$

This formula ensures that a perfect match (100 % accuracy) yields a score of 5, while the largest observed deviation results in a score closer to 2.

The overall fidelity score is calculated as the arithmetic mean of the fidelity scores for length, width, and height:

$$fidelity\ score = \frac{fidelity_{length} + fidelity_{width} + fidelity_{height}}{3} \quad (6)$$

Finally, the composite quality score (CQ) is calculated as the average of the visual score and the fidelity score:

$$CQ = \frac{print\ score + fidelity\ score}{2} \quad (7)$$

2.2.6. Texture analysis

Hardness of 3D printed snacks was assessed using TA.XTPlus Texture Analyser (Stable Micro Systems, Godalming, UK). The samples were placed into a three-point bending rig (HDP/3 PB) for snack cutting. The cutting position was shown in Fig. 2. Instrumental settings (project BIS2_KB) were derived from the sample projects of the software package (Texture Exponent Software TEE32, version 6.1.6.0., Stable Micro Systems) and a 50 kg loading cell was used. Hardness was quantified as the force needed to break the snack horizontally into two pieces (Belović et al., 2025). All measurements were conducted on five snacks.

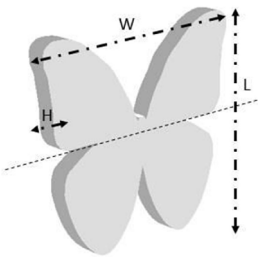

Fig. 2. 3D butterfly model with target dimensions (length (L) = 60 mm, width (W) = 60 mm and height (H) = 6 mm) and cross-sectional area indicating the cutting position for hardness measurements.

2.2.7. Data analysis

Statistical analysis was performed in Python (Jupyter Notebook) using the *pandas, scipy*, and *statsmodels* packages to examine the relationships between the experimental factors (I, EM, PS, and LH) and shape fidelity parameters (length, width, and height). Pearson correlation analysis was applied to evaluate linear associations between process parameters and dimensional fidelity responses, and the statistical significance of the obtained correlation coefficients was assessed using a two-tailed test ($p < 0.05$).

One-way analysis of variance (ANOVA), followed by Tukey's post-hoc test, was conducted to identify statistically significant differences among experimental runs. Compact letter display (CLD) was used to group runs according to statistically indistinguishable levels of deviation from target dimensional values.

Additionally, dimensional fidelity measurements were screened for statistically significant extreme observations using Grubbs' test ($\alpha = 0.05$), applied independently to length, width, and height fidelity data to distinguish between measurement anomalies and process-induced variability.

2.2.8. Artificial neural networks with genetic algorithm

The 3D printing process was optimized using a hybrid artificial neural network-genetic algorithm (ANN-GA) approach. The ANN effectively models nonlinear relationships, while GA serves as an optimization technique based on evolutionary principles (Livingstone, 2008; Carvajal-Mena et al., 2023).

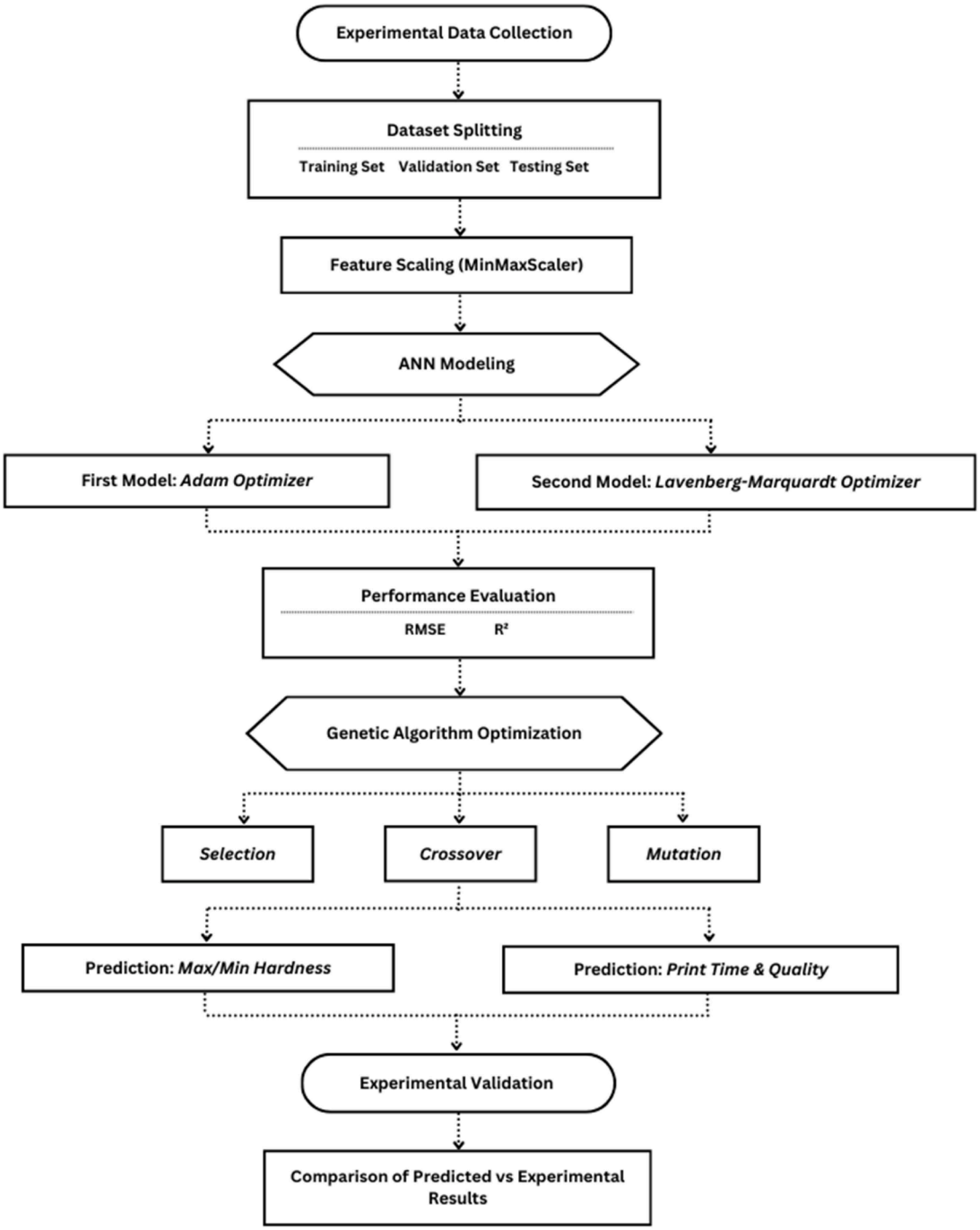

Fig. 3. Schematic representation of the ANN–GA modeling and optimization.

As shown in the Fig. 3, the workflow starts with experimental data collection, involving four input parameters: infill percentage (I), extrusion multiplier (EM), print speed (PS), and layer height (LH) - collected from 31 runs with 5 replicates each (155 datasets). Due to infeasible combinations (e.g., Runs 3, 12, 17, 18), 135 valid datasets were used. Dataset splitting was applied to produce training (70 %), validation (15 %), and test (15 %) sets, followed by feature scaling using MinMaxScaler.

Model development was done in Python (Jupyter Notebook) using relevant libraries for machine learning and optimization. Two ANN models were built using TensorFlow/Keras and Pyrenn libraries: (i) a predictive model for textural hardness, and (ii) an optimization model minimizing print duration while maintaining print quality (composite quality score).

The first neural network, consisting of three hidden layers, was trained using the Adam optimizer, while the second network had two hidden layers and was trained using the Levenberg–Marquardt algorithm. Model performance was evaluated using the coefficient of determination (R^2) and the root mean square error (RMSE), defined as (Jiao et al., 2024):

$$R^2 = 1 - \frac{\sum_{m=1}^{n}\left(y_{pre} - y_{act}\right)^2}{\sum_{m=1}^{n}\left(y_{pre} - y_{mean}\right)^2} \tag{8}$$

$$RMSE = \sqrt{\frac{\sum_{m=1}^{n}\left(y_{pre} - y_{act}\right)^2}{n}} \tag{9}$$

where y_{act} is the actual value, y_{mean} is the mean value, y_{pre} is the predicted value, and n corresponds to sample size.

The genetic algorithm optimization followed performance evaluation, addressing two distinct tasks: predicting input parameters for maximum or minimum hardness using the first ANN model, and balancing print time and quality using the second ANN model.

Additionally, the accuracy of the developed framework was tested and validated by using the following formula (Lee & Hashimoto, 2024):

$$Accuracy\ (\%) = \left(1 - \frac{|Predicted\ value - Measured\ value|}{Predicted\ value}\right) \times 100 \tag{10}$$

To assess the impact of input parameters on model outputs, sensitivity analysis was performed using permutation feature importance. For each input parameter, its values were randomly permuted, and the corresponding increase in model prediction error was quantified. The relative importance of each input was calculated as a percentage of the total error increase, providing a normalized measure of parameter influence within the model.

3. Results

3.1. Influence of input parameters on the print quality of 3D-Printed snacks

The calculated values for print and end-product quality responses corresponding to each combination of input variables are summarized in Table 2. All runs successfully achieved the intended butterfly shape, with varying degrees of dimensional accuracy, except for runs 3, 12, 17 and 18.

Shape fidelity is defined as the degree to which the designed geometry is reproduced with accuracy and consistency; the target value is 100 % in terms of length, width, and height. From Table 2 it can be seen that length fidelity measurements ranged from 98.57 ± 0.93 % to 107.87 ± 0.73 %. The most accurate length was obtained using 30 % infill, a low extrusion multiplier (60 %), low printing speed (10 mm/s), and the highest layer height (70 %) (Run 4). Conversely, the largest deviation was recorded for the combination of 50 % infill, 150 % extrusion multiplier, 15 mm/s printing speed, and 50 % layer height (Run 16).

In general, the best length fidelity (from 100.10 % to 102.01 %) was achieved using moderate extrusion (60–90 %), across all tested printing speeds (5–25 mm/s), and layer heights between 50 % and 70 %. When the extrusion multiplier increased beyond moderate values (> 90 %), structures became increasingly elongated due to over-extrusion. These trends align with the strong positive correlation between extrusion multiplier and length fidelity ($r = 0.80$) observed in Pearson correlation heatmap (Fig. 4). On the other hand, the combination of low extrusion multiplier, high printing speed, and high layer height resulted in undersized prints (length < target) (Run 1 and Run 13).

Similar trends were noted for width fidelity, which ranged from 99.72 ± 0.65 % to 107.32 ± 0.53 %. The most accurate width (99.72 ± 0.65 %) was achieved at a combination of low extrusion (60 %), high infill (70 %), high printing speed (20 mm/s), and high layer height (70 %) (Run 1). The largest deviation was again observed at maximum extrusion multiplier (Run 16), confirmed by positive correlation between extrusion and width fidelity ($r = 0.79$) indicating its dominant role.

Printing speed showed weak and statistically insignificant correlations with both width ($r = 0.08$) and length ($r = 0.03$). Infill percentage exhibited a weak but statistically significant negative correlation with width fidelity ($r = -0.17$), while its relationship with length remained insignificant. Layer height, however, showed significant moderate negative correlations with both width ($r = -0.30$) and length ($r = -0.21$) (marked with an asterisk in Fig. 4).

Height proved to be the most sensitive dimension, with fidelity ranging from 94.40 ± 2.43 % to 109.97 ± 1.49 %. The most accurate height was achieved using moderate values for all inputs (Run 28), while the greatest deviation from the target height occurred at the low layer height, where the final samples were significantly taller than expected (Run 28). Among the examined factors, extrusion multiplier showed a statistically significant moderate positive correlation with height fidelity ($r = 0.28$), whereas layer height exhibited the strongest statistically significant negative correlation ($r = -0.47$).

According to the compact letter display (CLD) obtained from Tukey's HSD test based on the overall deviation across all three dimensions (length, width, and height) (Table S1), the most accurate print was obtained using 50 % infill, an extrusion multiplier of 90 %, a printing speed of 15 mm/s, and a layer height of 50 % (Run 9). Conversely, the largest overall deviation was recorded for the combination of 50 % infill, 150 % extrusion multiplier, 15 mm/s printing speed, and 50 % layer height (Run 16). This evaluation across all three dimensions enables the identification of printing parameters that provide the highest overall dimensional stability of the structures after printing.

Unsuccessful runs 3 and 12 were observed when using a combination of high printing speed (20 mm/s), low extrusion multiplier (60 %), low layer height (30 %), and either 30 % or 70 % infill. In both cases, the printed structures failed during the printing process and could not maintain structural integrity.

Additionally, Runs 17 and 18 also resulted in unsuccessful prints. Compared to the central point combination, Run 17 and Run 18 differed in only one parameter each which is extrusion multiplier (30 %) and infill percentage (10 %), respectively. Despite the minimal parameter changes, both conditions resulted in failed prints.

To further illustrate variability in shape fidelity, a boxplot was created to show the measured fidelity for length, width, and height across all printed samples (Fig. 5). Length fidelity values ranged from 97 % to 105 %, with several outliers above 105 % and few below 97 %. The distribution was symmetric and centered on 101–102 %, indicating generally consistent reproduction of length dimensions with moderate variability. Width fidelity showed slightly higher median and mean value compared to length and also exhibited few outliers, particularly above upper quartile. Height fidelity, however, demonstrated the widest spread among all dimensions, with values ranging from 92 % up to over

115 %. While no outliers were present, the extended whiskers and larger interquartile range indicate high variability. The distribution was positively skewed, implying that in many cases final sample height exceeded target value.

To statistically verify whether the observed extreme values represented true outliers, Grubbs' test ($\alpha = 0.05$) was applied to the dimensional fidelity data. A statistically significant extreme observation (108.68 %) was detected in length fidelity, whereas no significant outliers were identified in width or height fidelity. The identified deviation was attributed to process-induced material accumulation during extrusion rather than measurement error. Consequently, this observation was retained in the dataset used for composite quality score (CQ) calculation in order to preserve inherent process variability and ensure that subsequent modelling reflects realistic printing behaviour.

3.2. *End-product quality*

Structural deformation of a product after post-processing is

Table 2
Experimental design variables with measured responses along with top and lateral view of printed samples.

Input parameters			Output parameters											
			Weight (g)		Shape fidelity (%)			Deformation (%)			Texture		Appearance	
Run	I:EM:PS:LH	Print time (min)	m_0	m_1	Length	Width	Height	Length	Width	Height	Hardness (N)	Print score	Top view	Lateral view
1	70:60:20:70	6.25	7.27 ±0.26	4.26 ±0.15	98.57 ±0.93	99.72 ±0.65	102.23 ±2.08	6.24 ±1.09	4.30 ±0.88	6.69 ±0.77	8.86. ±0.28	2.5		
2	70:120:10:70	12.14	14.66 ±0.70	10.09 ±0.33	102.68 ±0.22	103.18 ±0.50	97.63 ±1.56	3.44 ±0.56	3.88 ±0.77	-2.46 ±0.45	29.30 ±1.02	3		
3	30:60:20:30	10.20	/	/	/	/	/	/	/	/	/	1		
4	30:60:10:70	8.14	6.10 ±0.26	3.43 ±0.22	100.10 ±0.82	101.51 ±0.42	96.40 ±2.28	4.57± 0.92	4.82 ±0.55	5.36 ±0.61	5.17 ±0.42	4		
5	70:120:20:30	15	17.55 ±0.17	10.60 ±0.19	103.78 ±0.48	104.62 ±0.90	106.53 ±3.66	3.46 ±0.68	3.11 ±0.62	-2.43 ±0.41	37.92 ±2.42	3.75		
6	50:90:15:50	9.49	10.30 ±0.46	6.31 ±0.25	100.69 ±0.67	101.36 ±0.14	102.60 ±1.53	6.87 ±0.57	3.17 ±0.66	3.67 ±0.25	24.86 ±1.66	5		
7	50:90:15:50	9.49	10.11 ±0.59	6.32 ±0.46	101.32 ±0.77	102.69 ±0.80	101.87 ±3.29	3.79 ±0.69	3.53 ±0.50	3.28 ±0.56	24.90 ±1.42	5		
8	30:60:10:30	19.30	6.65 ±0.37	3.95 ±0.19	100.69 ±0.69	101.79 ±0.49	106.53 ±3.54	4.48 ±0.80	2.78 ±0.52	12.15 ±1.82	12.32 ±0,96	2		
9	50:90:15:50	9.49	10.28 ±0.15	6.24 ±0.23	101.72 ±1.17	102.48 ±0.47	96.00 ±1.03	4.36 ±0.68	2.11 ±0.37	1.46 ±0.27	25,17 ±0,85	5		
10	70:60:10:70	12.01	7.79 ±0.16	4.60 ±0.08	100.29 ±1.50	100.60 ±1.63	94.40 ±2.43	5.38 ±0.94	4.79 ±0.81	4.72 ±0.95	11,34 ±0,69	3		
11	50:90:5:50	27.55	9.28 ±0.10	5.52 ±0.19	100.22 ±0.28	100.56 ±0.22	97.77 ±1.19	4.81 ±0.81	4.61 ±0.51	3.28 ±0.33	27.54 ±0.85	5		
12	70:60:20:30	14.07	/	/	/	/	/	/	/	/	/	1		
13	30:60:20:70	4.22	5.37 ±0.32	3.18 ±0.20	98.60 ±0.93	100.73 ±0.62	96.70 ±2.18	4.23 ±0.65	1.29 ±0.24	12.38 ±2.02	3,38 ±0,11	2.5		
14	50:90:25:50	6	7.61 ±0.19	4.42 ±0.20	100.57 ±0.15	100.56 ±0.09	94.80 ±1.29	6.34 ±0.66	2.25 ±0.06	6.55 ±0.78	20.50 ±0.35	2		
15	30:120:20:70	4.29	10.75 ±0.19	6.52 ±0.12	101.54 ±0.69	103.67 ±0.60	102.67 ±1.25	4.22 ±0.71	2.92 ±0.25	3.80 ±0.32	17,51 ±0,31	5		

(*continued on next page*)

Table 2 (*continued*)

16	50:150:15:50	10	16.23 ±0.11	10.38 ±0.09	107.87 ±0.73	107.32 ±0.53	107.60 ±3.36	4.62 ±0.40	4.31 ±0.18	-6.83 ±1.23	34.69 ±0.88	3	
17	50:30:15:50	10	/	/	/	/	/	/	/	/	/	1	
18	10:90:15:50	6	/	/	/	/	/	/	/	/	/	1	
19	50:90:15:50	9.49	10.71 ±0.12	6.22 ±0.08	101.49 ±0.84	102.41 ±0.77	99.30 ±1.14	4.47 ±0.39	2.73 ±0.32	3.12 ±0.54	25,07 ±1,11	5	
20	30:120:10:70	8.16	10.55 ±0.17	6.24 ±0.11	102.22 ±0.66	103.75 ±1.14	102.73 ±5.24	4.87 ±0.41	2.79 ±0.50	7.80 ±0.89	16,74 ±0,73	4.25	
21	30:120:20:30	10.28	11.60 ±0.31	6.89 ±0.31	102.76 ±0.97	105.61 ±0.89	105.23 ±1.98	4.21 ±0.47	2.66 ±0.41	5.64 ±1.11	19,88 ±0,81	4	
22	30:120:10:30	19.44	11.72 ±0.16	7.65 ±0.13	103.13 ±0.97	105.27 ±0.98	106.37 ±1.78	4.78 ±0.08	3.05 ±0.38	6.21 ±0.64	27,76 ±1,28	4	
23	70:120:10:30	28.57	17.34 ±0.36	11.68 ±0.23	102.33 ±0.68	102.68 ±1.02	106.23 ±5.53	4.41 ±0.49	3.47 ±0.35	-7.97 ±0.73	38,62 ±1,05	4	
24	50:90:15:90	5.51	9.60 ±0.18	5.78 ±0.13	101.21 ±0.35	101.97 ±0.28	106.07 ±3.74	4.68 ±0.21	2.46 ±0.13	13.39 ±1.05	14.83 ±0.94	3	
25	50:90:15:50	9.49	10.54 ±0.05	6.40 ±0.08	102.01 ±0.45	102.70 ±0.75	96.40 ±1.94	5.29 ±0.68	3.34 ±0.66	-1.63 ±0.26	22,45 ±0,97	5	
26	70:120:20:70	6.50	14.98 ±0.19	9.08 ±0.27	104.17 ±0.66	104.40 ±0.52	100.70 ±1.40	4.97 ±0.45	3.98 ±0.43	-8.27 ±1.36	33,76 ±3,98	3.5	
27	70:60:10:30	28.40	9.56 ±0.53	5.63 ±0.21	100.64 ±0.85	101.57 ±0.35	108.90± 0.96	4.83 ±0.83	4.75 ±0.94	13.07 ±2.25	12,61 ±1,44	2	
28	50:90:15:50	9.49	9.83 ±0.21	5.75 ±0.14	100.84 ±0.21	102.27 ±0.40	99.40 ±1.81	4.59 ±0.88	3.75 ±0.56	1.61 ±0.29	24,00 ±1,35	5	
29	50:90:15:10	50.33	12.51 ±0.14	8.28 ±0.12	101.78 ±0.36	104.06 ±0.53	109.97 ±1.49	5.75 ±0.70	2.76 ±0.63	2.21 ±0.47	27.71 ±1.27	2.5	
30	90:90:15:50	13.45	15.75 ±0.09	10.54 ±0.14	101.66 ±0.16	101.98 ±0.17	103.80 ±1.98	4.47 ±0.20	2.76 ±0.15	2.31 ±0.45	37.08 ±0.89	4	
31	50:90:15:50	9.49	10.40 ±0.43	6.19 ±0.38	101.72 ±0.45	102.07 ±0.39	102.90 ±2.37	4.91 ±0.83	3.82 ±0.62	3.49 ±0.58	23,43 ±1,69	5	

I-infill (%), *EM*-extrusion multiplier (%), *PS*-print speed (mm/s), *LH*-layer height (% of nozzle diameter), m_0-weight of samples after printing, m_1-weight of samples after post-processing. One-way ANOVA indicated statistically significant differences among experimental runs in terms of dimensional fidelity, post-processing deformation, and hardness ($p < 0.05$).

estimated as a change of its dimensions in comparison to a printed product. Positive value indicates shrinkage, while a negative value implies spreading of sample (Mustač et al., 2023). The dried samples successfully preserved the overall shape and structural features of the original design, demonstrating good stability after post-processing. However, inevitable deformations of 3D-printed structures after post-processing can be observed. Length and width deformation reached up to 6.87 ± 0.57 % and 4.82 ± 0.55 %, respectively, which are in the range reported in literature.

Height deformation showed a wider range, from −8.27 ± 1.36 % expansion (Run 26) to 13.39 ± 1.05 % shrinkage (Run 24). Height expansion was observed in several samples (e.g. Runs 2, 5, 16, 23, 25, and 26). These samples shared common printing conditions, moderate to high infill levels (50–70 %) combined with high extrusion (120–150 %), indicating greater solid fraction and mass.

According to the compact letter display (CLD) derived from Tukey's HSD test based on the overall deviation from the target deformation value (0 %), calculated across all three dimensions (length, width, and height) (Table S2), Runs 26, 23, and 16 formed the statistically superior group, exhibiting the lowest overall structural distortion after thermal post-processing. In contrast, Runs 8, 24, and 27 showed significantly higher deformations. This combined analysis allowed identification of the printing conditions that produced the most dimensionally stable structures after drying.

Baking loss is another important quality parameter reflecting the extent of water and other components loss during thermal post-

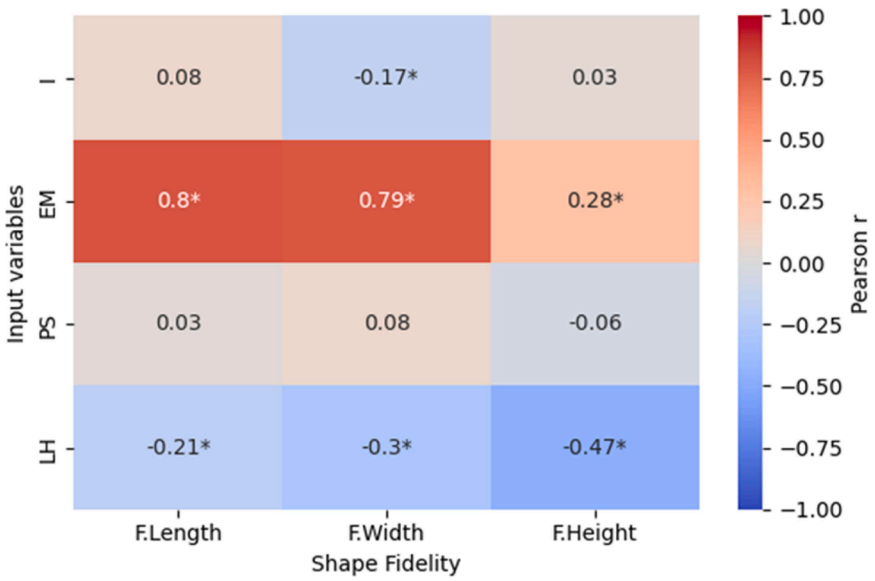

Fig. 4. Pearson correlation heatmap showing the relationship between input variables (I: infill, EM: extrusion multiplier, PS: printing speed, and LH: layer height) and shape fidelity (length, width, and height). Statistically significant correlations ($p < 0.05$) are indicated by an asterisk (*).

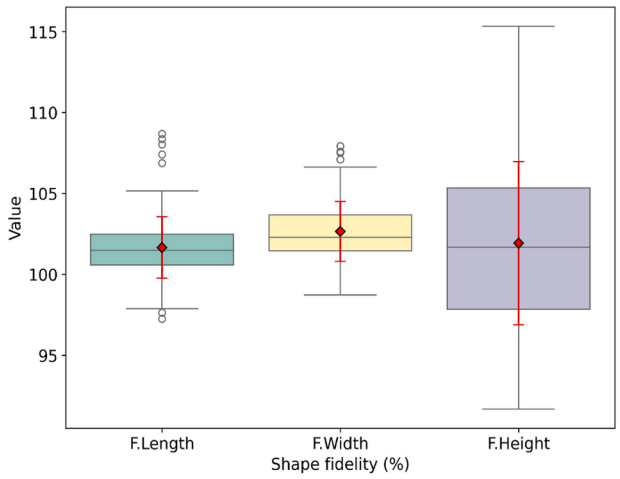

Fig. 5. Boxplot showing shape fidelity (%) of printed snacks in three dimensions: length, width, and height.

processing, such as baking (Mudau & Adebo, 2024). The calculated baking loss of 3D-printed snacks ranged from 31.17 % to 43.77 %, with a mean value of 38.92 % (Fig. 6). These values indicate a relatively high level of water loss. The highest moisture loss was observed in Run 4 (43.77 %), while the lowest moisture loss occurred in Run 2 (31.17 %).

Notably, most samples exhibited moisture losses ranging between 39 % and 41 %, indicating good consistency and uniform heating, reinforcing the reliability of the selected baking settings.

3.3. Optimizing print time and quality using ANN-GA

Another phase of this research focuses on optimizing the printing parameters to achieve efficient, high-quality 3D printing by balancing print time and print quality (represented by the composite quality score). Since the experimental phase had already yielded a satisfactory level of performance (CQ scores between 4 and 5), the optimization effort was aimed at reducing print time while maintaining those results. Our approach gave a slight advantage to minimizing duration, exploring how much the process could be shortened without compromising the snack's appearance or structural integrity.

To this end, a hybrid ANN-GA model was employed to determine the optimal set of printing parameters capable of achieving this balance. As shown in Table 3, the coefficient of determination (R^2) values for the training, validation, and testing datasets ranged between 0.9748 and 0.9997 for all predicted variables, indicating excellent model fit. Furthermore, the root mean square error (RMSE) for predicting print time (expressed in seconds) ranged from 8.57 to 20.01, while for CQ score it ranged between 0.053 and 0.088. The combination of high R^2 values and minimal RMSE confirms the outstanding predictive performance of the ANN-GA model. These results directly support the main goal of the study—to significantly shorten the printing process while preserving the quality and texture of the final product, thereby justifying the need for optimization and demonstrating its effectiveness for future commercial applications.

The measured and predicted print time values and printing scores are shown in Fig. 7. The prediction model for print time performed well with R^2 value of 1 (Fig. 7a), whereas the R^2 value of linear fitting for predicted and measured CQ score was 0.988 (Fig. 7b). These results confirm that both print time and print score can be accurately predicted by the ANN-GA model based on the selected input printing parameters.

Fig. 8 presents the sensitivity analysis of the ANN-GA model for print time and CQ score. For print time, LH exhibited the strongest negative influence, followed by PS, which also showed a negative effect. Positive influence on print time showed I, while EM had the least impact among the analyzed parameters. Regarding the CQ score, EM showed the strongest positive influence, followed by LH, which also contributed positively. PS exhibited a moderate negative effect on the CQ score, whereas I had only a minor influence.

The ANN-GA model was employed to identify the optimal combination of parameters that minimizes print time while maintaining a high level of print quality within the desirable range of 4–5. Under optimal conditions (I:EM:PS:LH = 30:120:25:90), the model predicted a CQ score of 4.87 and a total print time of 3 min and 31 s.

According to the literature, print quality and print time are inherently conflicting objectives - improving one often comes at the expense of the other (Derossi et al., 2019). Nevertheless, the developed model effectively minimized this trade-off, offering a time-efficient solution without compromising acceptable print quality. Based on Eq. (10), the prediction accuracies presented in Table 4 were 85.30 % for print time and 95.89 % for the CQ score. Interestingly, the experimental results demonstrated an even shorter print time and a slightly lower quality

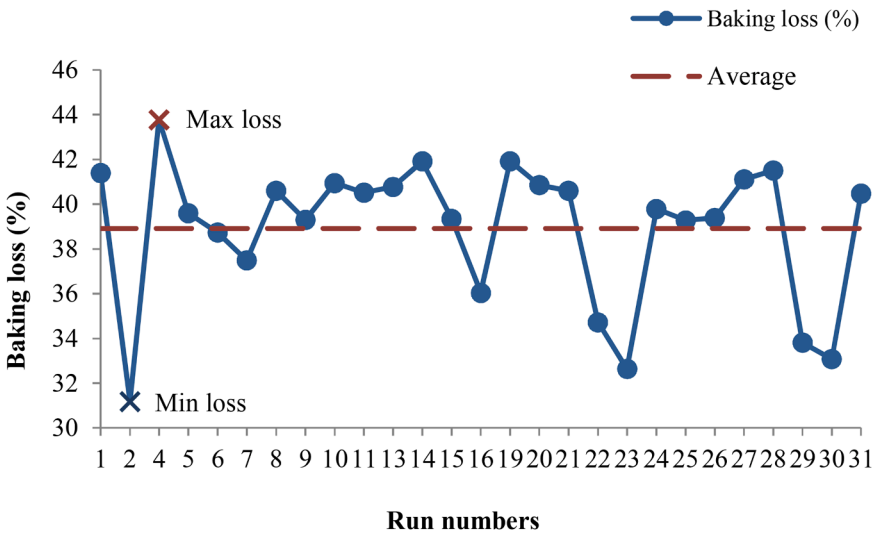

Fig. 6. Line chart showing the percentage of moisture loss across 31 different samples of 3D-printed cereal-based snacks.

Table 3
Performance metrics of the ANN-GA model for predicting print time and CQ score of 3D printed snacks based on printing parameters.

Predicted variable	R^2			RMSE		
	Training	Validation	Test	Training	Validation	Test
Print time	0.9997	0.9996	0.9990	10.7676	8.5679	20.0103
CQ score	0.9895	0.9748	0.9917	0.0590	0.0881	0.0530

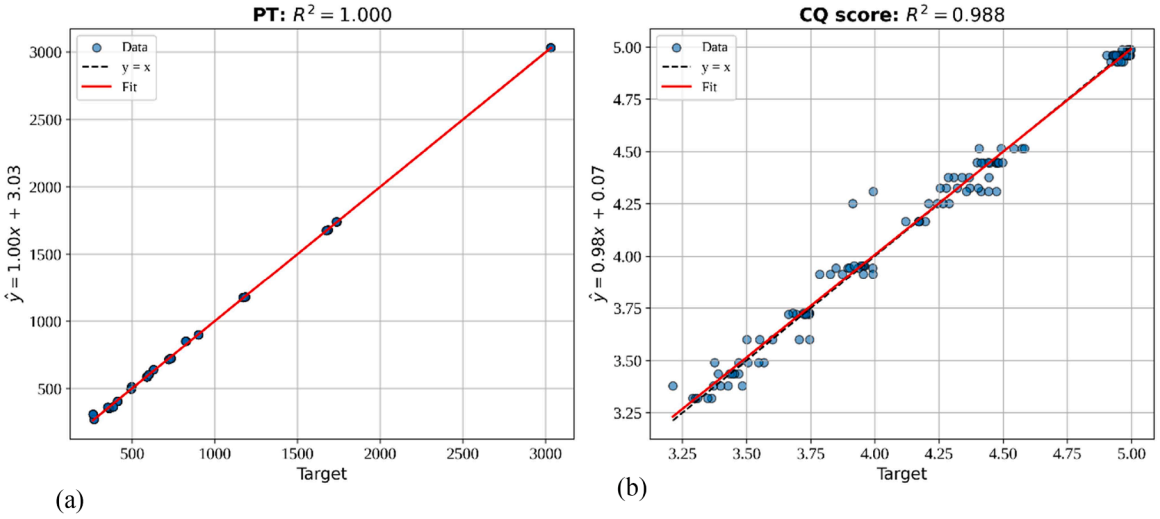

Fig. 7. Measured and predicted values for print time (a); CQ score (b).

score than those predicted by the model.

The best experimental outcome was observed in Run 15, with a print time of 4 min and 29 s and a quality score of 4.59 (Table 2). In comparison, the optimal conditions determined by the ANN-GA model succeeded in reducing print time by 1 min and 29 s while achieving an even slightly higher quality score. These findings confirm that the ANN-GA model is a powerful tool for optimizing 3D printing processes, enabling significant improvements in efficiency without sacrificing product quality.

3.4. Modelling and optimization of texture profile in 3D-Printed snacks

The structures were printed based on the CCD design (Table 1) and the hardness was evaluated (Table 2). The data, including I, EM, PS and LH were respectively defined as input variables for predicting the minimum and maximum hardness of the printed snacks. From Table 5, it was observed that the model achieved R^2 values ranging from 0.968 to 0.981, indicating a strong degree of fitting. Additionally, the RMSE values for predicting hardness (1.271–1.903) further confirmed the model's good predictive performance.

Fig. 9 represents the fitting plots of the ANN-GA model for training, validation, and test datasets, as well as for all data combined with an overall R^2 value as 0.977. This result indicated that the established model exhibited good performance and was suitable for prediction of the hardness through the printing parameters (I, EM, PS and LH) as the input signals.

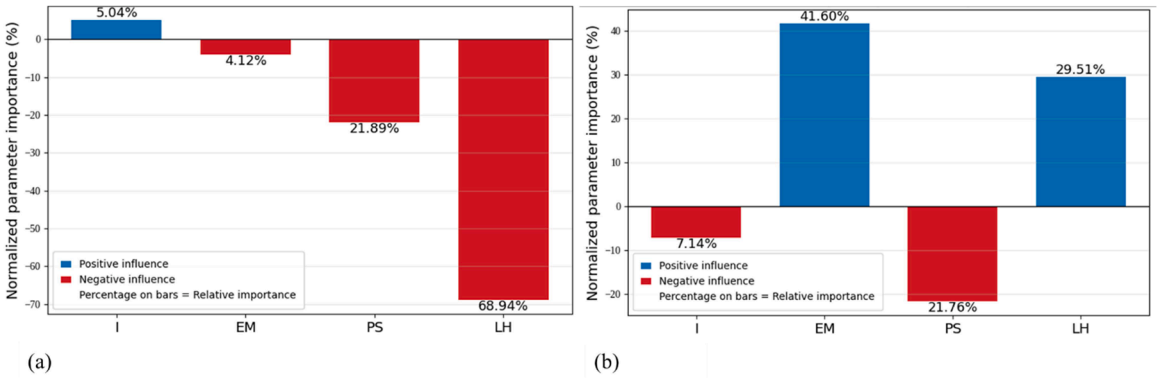

Fig. 8. Sensitivity analysis of the ANN-GA model for print time (a) and CQ score (b).

Table 4
Comparison of predicted and measured responses.

Response	Predicted value	Measured value	Accuracy (%)	Appearance	
				Top view	Lateral view
Print time	3.31	3.00	85.30		
CQ score	4.87	4.67	95.89		

The hardness of 3D snacks measured by three-point bending test varied from 3.38 N (Run13, Table S3) to 38.62 N (Run 23, Table S3). Printing parameters responsible for the softest snacks are lowest I, lowest EM, highest PS and highest LH (I:EM:PS:LH = 30:60:20:70). Fig. 10 presents the results of the sensitivity analysis evaluating the predictive influence of the input neurons. The analysis reveals that the EM was the most influential factor, contributing 60.89 %, followed by I at 27.18 %, LH at 8.86 %, and PS with the least impact at 3.08 %. A positive influence was found between EM and hardness (60.89 %), indicating that higher EM leads to increased hardness. The increase in hardness was more pronounced when the EM increased from 60 % to 80 %, while further increases (80–120 %) resulted in a less steep rise in hardness (Table 2). Infill also showed a positive association with hardness, with higher infill levels (from 30 % to 70 %) leading to increased hardness values. In contrast, PS and LH exhibited negative associations with hardness, with LH showing a stronger negative effect than PS. The influence of PS on hardness was minimal across the tested range.

The use of the ANN-GA model allows for the identification of the optimal combination of independent variables that predicts hardness. For example, the predicted minimum and maximum hardness were 3.2 N and 64.07 N, respectively. The required parameters to establish the minimum and maximum hardness were (I:EM:PS:LH = 30:30:5:70) and (I:EM:PS:LH = 90:150:5:10), as shown in Table 6.

The first run aimed to replicate the minimum hardness, while the second targeted the maximum. Based on the results presented in Table 7, it can be concluded that the developed model accurately predicted hardness values of 3.2 N and 64.25 N, achieving prediction accuracies of 96.25 % and 93.48 %, respectively, as calculated according to Eq. (10).

Table 5
Performance parameters of ANN-GA model predicting hardness of baked 3D snacks based on printing parameters data.

Predicted variable	R^2			RMSE		
	Training	Validation	Test	Training	Validation	Test
Hardness	0.981	0.970	0.968	1.271	1.903	1.650

4. Discussion

4.1. Influence of key printing parameters on product quality and process performance

The obtained results demonstrate that shape fidelity, print quality, textural properties, and production efficiency of 3D-printed cereal-based snacks are primarily governed by extrusion multiplier and layer height, while printing speed and infill percentage act as secondary but strongly interacting parameters. Rather than operating independently, these variables exhibit combined effects that define the balance between shape accuracy, structural integrity, and texture.

EM emerged as the dominant parameter influencing dimensional fidelity, print quality, and hardness. Its strong positive correlation with length and width fidelity confirms that excessive material deposition directly causes dimensional enlargement and reduces precision. Similar behavior was reported by Pradhan et al. (2025), who showed that over-extrusion degrades shape accuracy, with printing precision deviations exceeding 100 % at the highest extrusion rate. Conversely, insufficient extrusion resulted in under-filled layers, poor interlayer cohesion, and print failures, particularly when combined with high printing speeds or extreme infill values. These observations align with studies on chocolate (Hao et al., 2010) and food paste printing (Liu & Ciftci, 2021), which highlight the necessity of balancing material flow and nozzle movement. Liu & Ciftci (2021) demonstrated that increasing printing speed without a proportional increase in extrusion rate leads to inadequate material supply, resulting in reduced print quality. Similarly, Hao et al. (2010) reported that higher nozzle movement speeds at a constant extrusion rate elongate the extruded filament, as the same material volume is distributed over a larger surface area, reducing line width and compromising deposition uniformity.

The dominance of extrusion multiplier (EM) observed in this study can be explained by its fundamental role in controlling material flow during the extrusion process. From a physical standpoint, EM directly regulates the volumetric flow rate of the material exiting the nozzle, determining the amount of material deposited per unit length of the printing path. Consequently, variations in EM modify the cross-sectional area of the deposited filament and significantly affect the geometry and

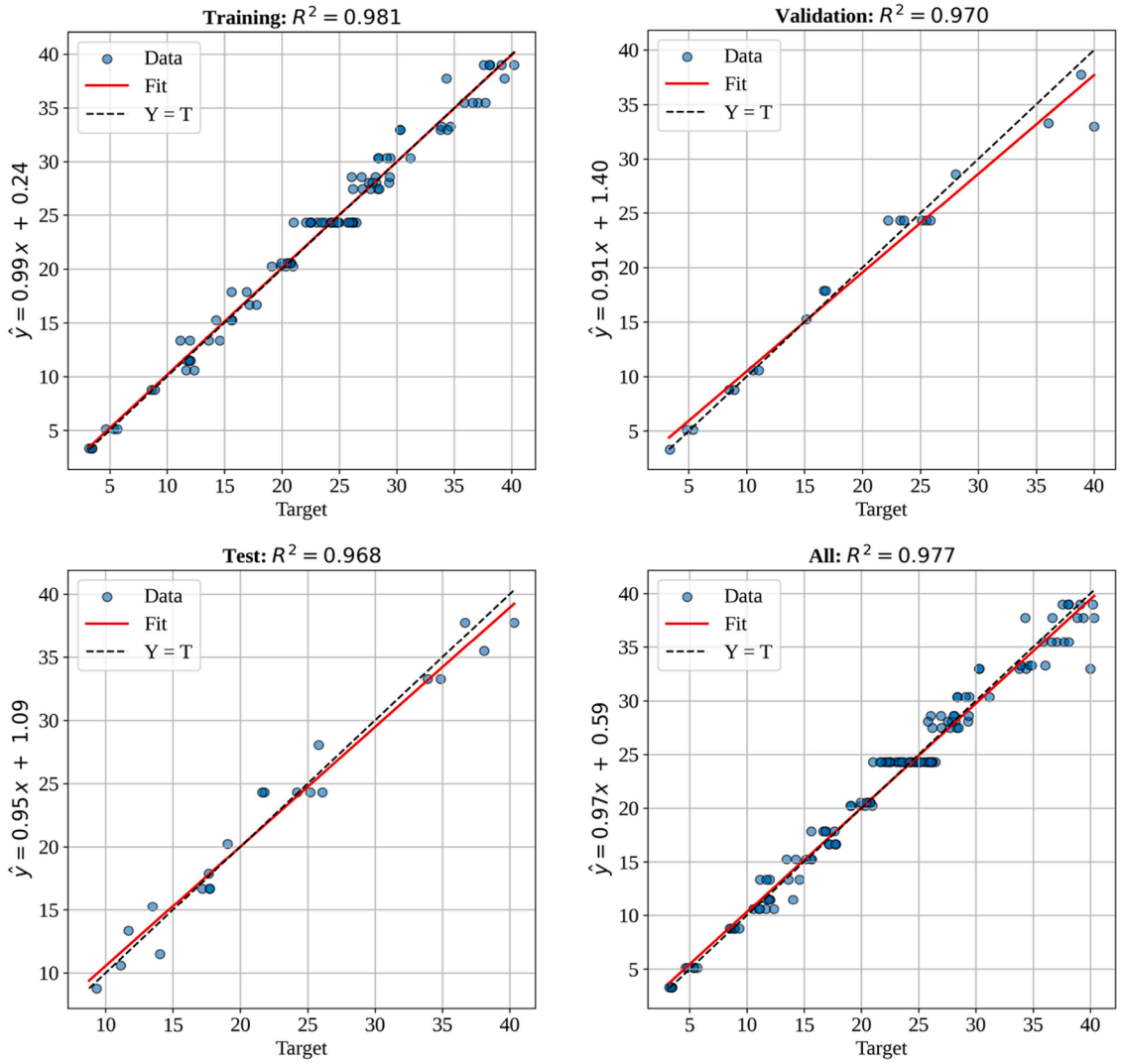

Fig. 9. Fitting graph of ANN-GA model predicting hardness of baked 3D snacks based on printing parameters data.

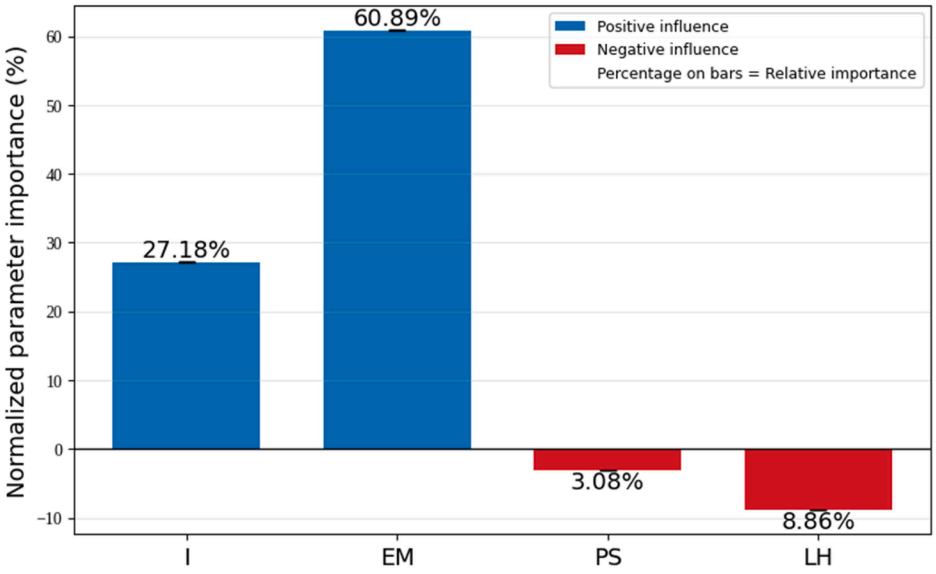

Fig. 10. Sensitivity analysis of the ANN-GA model for predicting the hardness of baked 3D snacks.

Table 6
Predicted boundaries of responses with corresponding parameters.

	Range		Min. level settings				Max. level settings			
Response	Min	Max	I (%)	EM (%)	PS (mm/s)	LH (%)	I (%)	EM (%)	PS (mm/s)	LH (%)
Hardness (N)	3.20	64.25	30	30	5	70	90	150	5	10

Table 7
Comparison of predicted and measured responses.

Response	Predicted value		Measured value		Accuracy (%)		Appearance		
	Min	Max	Min	Max	Min	Max		Min	Max
Hardness (N)	3.2	64.25	3.02	60.06	96.25	93.48	Top view		
							Lateral view		

density of the printed structure (Sadaf et al., 2022). In extrusion-based additive manufacturing, stable deposition requires a balance between the volumetric flow rate and the nozzle movement speed (Equbal et al., 2024). When extrusion exceeds the material demand defined by the printing path, excess material accumulates, leading to filament spreading, dimensional deviation, and increased structural density and fewer printing voids. Conversely, insufficient extrusion produces thin or discontinuous filaments, resulting in weak interlayer bonding, formation of large void fractions and poor structural stability (Sadaf et al., 2022; Loskot et al., 2023). These mechanisms reflect the fundamental fluid-mechanical relationship between material flow rate and velocity that governs filament formation and dimensional accuracy in extrusion-based printing systems.

LH proved to be the most critical parameter for height fidelity, confirming that vertical accuracy is more sensitive than planar dimensions. The strong negative correlation between LH and printed height is consistent with the observations of Severini et al. (2016), who reported that increased LH reduces stacking stability and promotes layer sagging. At high LH, irregular layer placement accumulates throughout the structure, progressively reducing final height (Run 10; Table 2). In contrast, very low LH leads to excessive vertical growth (Run 29; Table 2). This can be explained by extrudate swell effect and material build-up caused by high extrusion pressure and close nozzle proximity to a previously deposited layer, as described by Oyinloye and Yoon (2021). This effect is further amplified by the increased number of layers, where small deviations accumulate into dimensional errors. This observation was also noted by Yang et al. (2019), stating that the small changes in each layer will cause the large cumulative change. These findings collectively emphasize that slicer-defined nominal heights must be experimentally calibrated rather than assumed, accounting for the interaction between layer height, extrusion rate, and nozzle diameter (Guo et al., 2019).

PS and I exhibited relatively weak direct correlations with external dimensions, which is consistent with previous reports indicating that PS predominantly affects print time and mass flow ($p < 0.001$) rather than geometric deformation (Barrios-Rodríguez et al., 2024). Similarly, infill primarily modifies the internal structure of the printed object, with only a minor influence on external geometry, as changes in infill from 10 to 20 % were reported to induce a maximum diameter variation of approximately 1 mm (Severini et al., 2016). However, their interaction with extrusion multiplier proved critical. High PS combined with low extrusion resulted in insufficient material deposition, leading to fragile structures at low infill (e.g. Run 3 and 12; Table 2) and unstable, under-filled layers at high infill (e.g. Run 13; Table 2) since the material demand exceeded low extrusion rates. These failures indicate that EM and I must remain above a critical threshold to ensure dimensional stability and successful printing.

Production efficiency, particularly print time, remains a crucial factor for scaling 3D food printing beyond laboratory applications (Arora & Prithviraj, 2022). LH showed the strongest influence on print time, as decreasing LH increases the number of deposited layers and prolongs printing process. This effect was evident for example in Runs 15 and 21 where reduced LH (from 70 % to 30 %) resulted in and approximately 2.4 fold increase in printing time (from 4,29 to 10,28 min). These findings are in agreement with previous reports stating that by using a small layer height, the printing time significantly increases as well as the amount of food material used to print the whole 3D structure (Pradhan et al., 2025; Derossi et al., 2019). High PS reduced print time, while high I increased print duration due to greater material deposition and nozzle movement requirements. This observation is consistent with previous findings by (Huang et al., 2019) showing that both infill density and the number of perimeters positively contribute to printing time, indicating that print duration can be effectively shortened by reducing infill density. Notably, EM had minimal influence on print time, indicating that nozzle motion rather than extrusion volume is the primary determinant of printing duration.

Mechanical properties, particularly hardness, were predominantly controlled by EM and infill density.

Extrusion rate directly affects the internal packing density of the printed strands meaning that higher extrusion levels increase filament thickness and interlayer contact area (Sadaf et al., 2022). Increased extrusion and higher infill levels produced denser internal structures with reduced void fractions, resulting in higher hardness values, consistent with observations reported for carbohydrate-rich snacks (Usman et al., 2025), soy protein-based systems (Carranza et al., 2023), and air-fried products (Feng et al., 2020). However, low hardness did not necessarily correspond to optimal dimensional stability as insufficient extrusion combined with high PS led to poor layer adhesion and increased deformation, diverging from trends reported by Pradhan et al. (2025). This highlights that softness alone cannot be used as a quality indicator without considering print fidelity.

LH and PS exhibited weak but negative associations with hardness, confirming that higher LH and excessive speeds reduce material compaction and interlayer bonding. The combined effects of these parameters have also been reported by Lee & Hashimoto (2024), who showed that appropriate combinations of speed and layer height can either reduce or enhance hardness depending on deposition efficiency and void formation. In particular, Zhang et al. (2024) showed that printed structures retained comparable integrity at moderate nozzle speeds, whereas excessively high printing speeds (over 50 mm/s) caused

filament breakage and reduced shape fidelity due to dragging effects, which is consistent with the reduced compaction and weaker layer adhesion observed in the present study. Furthermore, reducing LH increases printing time and material compaction, indirectly contributing to increased hardness (Wu, 2018). Overall, achieving optimal texture therefore requires careful synchronization of movement speed and extrusion rate to avoid over- or under-deposition and ensure uniform structure formation.

Dimensional changes observed after thermal post-processing further reflect the influence of internal structure created during the printing stage. Thermal treatments such as cooking, drying, steaming, or baking are commonly applied to cereal-based printed systems to improve their sensory and nutritional characteristics, but maintaining structural integrity during these processes remains a key challenge for practical applications of food 3D printing (Severini et al., 2016; Radoš et al., 2023a; Thangalakshmi et al., 2022; Habuš et al., 2021).

In the present study, the printed snacks generally maintained their original geometry after drying, indicating good structural stability of the developed formulation. Nevertheless, moderate dimensional deformations were observed, which is consistent with previous studies on cereal-based printed products. Radoš et al. (2023a) reported dimensional deviations of up to approximately 10–12 % during oven drying of 3D-printed cereal structures.

Vertical deformation proved to be the most variable parameter during post-processing. Deng et al. (2023) and Feng et al. (2020) demonstrated that hot-air drying can cause significant shrinkage of printed food structures, with height reductions reaching up to 21 % and 15 %, respectively. These observations support the widely accepted mechanism that rapid moisture evaporation induces structural contraction and collapse of internal pores.

Interestingly, expansion of printed samples in the vertical direction was also observed under certain printing conditions. Samples printed with higher infill levels (50–70 %) and extrusion multipliers (120–150 %) exhibited height expansion after drying, consistent with the findings of Guénard-Lampron et al. (2021), who reported that higher fill rates (40–100 %) lead to greater mass after printing and increased height (swelling) and width deformation after baking. Rapid surface moisture loss during drying promotes crust formation, which traps steam inside the structure and generates internal pressure, causing expansion particularly in denser samples with fewer voids (Krishnaraj et al., 2019). These results highlight that internal density not only affects mechanical properties but also governs dimensional changes during thermal treatment.

Understanding baking loss is crucial, as it directly influences the texture, shelf life, and structural stability of 3D-printed snacks, thereby playing a key role in both product quality and consumer acceptability (Kadival et al., 2023). The baking loss values observed in this study further supports previously stated observations. Structures with lower infill and extrusion levels, which contain higher void fractions, facilitate faster moisture diffusion and exhibit greater mass loss during baking. Conversely, denser structures formed at higher infill and extrusion levels can act as a barrier to moisture migration, slowing dehydration during thermal processing. Such behavior illustrates the combined influence of printing parameters and internal microstructure on post-processing outcomes.

Overall, the findings demonstrate that extrusion multiplier and layer height are the primary drivers of dimensional accuracy, structural integrity, and textural behaviour, while printing speed and infill modulate these effects through strong interactions. Successful 3D printing of cereal-based snacks thus depends on balancing these parameters rather than optimizing them individually, reinforcing the importance of integrated process optimization strategies.

4.3. ANN–GA optimization and practical implications for 3D food printing

The inherent trade-off between print quality and print time is widely acknowledged in 3D food printing (Liu et al., 2017: Perez et al., 2019; Derossi et al., 2020). In this study, the hybrid ANN-GA model successfully navigated this conflict by identifying parameter combinations that significantly reduced print time while maintaining acceptable quality. The optimized conditions achieved a print time reduction of approximately 33 % compared to the best experimental run, without compromising the CQ score range required for visual and structural acceptability. From a practical perspective, such reduction in printing time has important implications for energy efficiency, throughput, and scalability of 3D food printing systems (Liu et al., 2017).

Importantly, preliminary laboratory-scale cost benchmarking indicated that the optimized printing strategy operates within a realistic and feasible cost range under experimental conditions (Simeunović et al. 2025). In this context, the approximately 33 % reduction in print time achieved through ANN–GA optimization represents a meaningful improvement in processing efficiency, supporting the potential of the proposed approach for future scale-up and industrial application.

Achieving a substantial reduction in printing time without compromising product quality contributes directly to Sustainable Development Goal 9 (Industry, Innovation and Infrastructure) by enhancing advanced manufacturing technologies, and SDG 12 (Responsible Consumption and Production) by promoting energy-efficient and resource-optimized food production systems (Derossi et al., 2024). Although the optimized CQ score was slightly lower than the maximum observed experimentally, this difference is unlikely to substantially affect consumer perception, particularly when balanced against gains in production efficiency. Under the optimized printing conditions, the snacks exhibited well-defined geometries, uniform layer deposition, and balanced textural attributes, features that are widely recognized as critical determinants of consumer acceptance in 3D-printed foods. These observations are in agreement with our previous findings (Simeunović et al., 2025), where millet-based formulations printed under comparable parameter settings achieved favorable sensory scores for both appearance and texture. This consistency confirms that improved shape fidelity and controlled hardness are directly linked to enhanced visual appeal and mouthfeel.

The use of an ANN-GA hybrid model in this study proved effective for simultaneously optimizing multiple objectives in 3D food printing, namely print time and print quality (CQ) score. Compared to traditional Response Surface Methodology (RSM), ANN-GA offers several advantages in the context of complex, non-linear interactions among printing parameters (Carvajal-Mena, et al., 2023). The prediction accuracy of the ANN-GA model was high, with R^2 values of 95.89 % for CQ score and 85.30 % for print time, indicating strong agreement between predicted and experimental results. These findings are consistent with previous food printing studies, such as Jiao et al. (2024) and Carvajal-Mena et al. (2023). In our study, the model successfully captured the dominant influence of extrusion multiplier on print quality, the primary effect of layer height on print time, and the secondary roles of infill and speed, highlighting its ability to reflect the complex, non-linear interactions among parameters that were also evident in the experimental data.

Carvajal-Mena et al. (2023) demonstrated that ANN–GA achieved $R^2 = 99.98$ % in predicting multiple quality responses for salmon gelatin 3D printing, significantly outperforming RSM ($R^2 = 93.99$ %) indicating a substantially better fit to the experimental data and more accurate prediction of multiple quality outcomes. This higher predictive fidelity supports the choice of ANN–GA for systems with strong nonlinearity and multiple interdependent responses. Jiao et al. (2024) employed a BP-ANN model to predict printability and rheological behavior of starch-based inks and reported strong predictive performance, confirming the suitability of ANN for modeling complex food printing systems. However, their approach focused exclusively on prediction,

without integrating a global optimization strategy. In comparison, the ANN-GA framework used in the present study demonstrated practical utility beyond prediction: it identified optimal parameter combinations (I:EM:PS:LH = 30:120:25:90) that reduced print time and maintained high CQ scores, surpassing the performance of individual experimental runs. This emphasizes the model's advantage for 3D food printing applications, where balancing efficiency, structural fidelity, and sensory quality is critical (Derossi et al., 2020).

Despite the promising outcomes, certain limitations of this study should be acknowledged. The findings are based on a single gluten-free dough formulation and one geometric design, which may influence their broader applicability. Nevertheless, these conditions provide a clear foundation for future research, which could explore a wider range of formulations, more complex geometries, and additional post-processing methods. Furthermore, the integration of the ANN–GA framework into real-time process control systems represents a promising avenue for further enhancing the industrial relevance of 3D food printing.

5. Conclusions

In this study, the combined effects of infill percentage, extrusion multiplier, printing speed, and layer height on the print quality and texture of gluten-free millet-based snacks enriched with almond and yeast powder were investigated. The study revealed that the extrusion multiplier (EM) is the most influential printing parameter affecting dimensional fidelity, showing positive correlations with length and width accuracy ($r \approx 0.80$), where higher EM values generally improve precision but may cause over-extrusion and elongation if excessive. Layer height (LH) negatively impacted height fidelity ($r = -0.47$) and hardness, while very low LH caused excessive vertical growth due to material build-up. Infill percentage (I) moderately influenced print quality and hardness, with higher infill levels increasing structural density and hardness up to 38.62 N, but also contributing to moisture retention and baking loss ranging from 31.17 % to 43.77 %. Print speed (PS) had minimal effects on shape fidelity and hardness, though very high speeds (20–25 mm/s) combined with low EM caused print failures from insufficient material deposition. Post-processing drying preserved shape with minimal length and width deformation, but height showed the greatest variability, with puffing causing expansions. The ANN–GA model successfully predicted hardness with high accuracy and identified EM and I as key positive contributors, while LH and PS negatively influenced hardness. ANN–GA optimization reduced print time by 33 %, from 4 min 29 s to 3 min, while maintaining quality (CQ score ~4.67). Finally, the complex butterfly design revealed dimensional instability at curved regions, underscoring the necessity of parameter optimization, which was effectively accomplished through ANN–GA modelling to achieve high shape fidelity, optimal hardness, and balanced baking time.

From an application perspective, these findings enable the definition of formulation-specific process windows for extrusion-based 3D printing of millet-based snacks. It should be noted that optimal parameter settings in 3D food printing are strongly dependent on material rheology and printer configuration; therefore, the recommended operational ranges are not universally applicable but reflect the behaviour of the investigated formulation under the applied system conditions. To achieve high-precision printing and dimensional stability, the extrusion multiplier (EM) is recommended to be maintained within the range of 90–120 %, ensuring sufficient material deposition for consistent interlayer bonding without inducing over-extrusion-related dimensional enlargement. In addition, layer height (LH) should be kept below 50 % of the nozzle diameter to minimize vertical expansion caused by material accumulation and extrudate swell effects. Printing speeds up to 20 mm/s were found to have limited influence on hardness and dimensional fidelity when appropriate extrusion levels were applied; however, higher speeds combined with low EM increased the risk of under-extrusion and structural collapse. Infill levels between 30 and 50 % provided a suitable balance between mechanical strength and post-processing deformation. These findings suggest that successful printing performance is governed by synchronized control of material flow and nozzle movement rather than independent optimization of individual parameters.

Ethical statement - studies in humans and animals

The authors declare that this study did not involve Humans or Animals

CRediT authorship contribution statement

Lidija Perović: Writing – original draft, Investigation, Formal analysis. **Jovana Simeunović:** Writing – original draft, Investigation, Data curation. **Jelena Jovančević:** Validation, Formal analysis, Data curation. **Jelena Miljanić:** Writing – review & editing, Writing – original draft, Conceptualization. **Bojana Kokić:** Visualization, Supervision, Resources. **Slobodan Birgermajer:** Visualization, Software, Methodology. **Predrag Kojić:** Visualization, Software, Data curation. **Jovana Kojić:** Writing – review & editing, Supervision, Project administration, Conceptualization.

Declaration of competing interest

The authors state that they have no financial or personal conflicts of interest that could have influenced the research presented in this paper.

Acknowledgements

This research was conducted within the Proof of Concept project: CeReal-basEd 3D PRINTED Snacks with Plant Proteins – REPRINT3D, provided by SAIGE. Current research was funded by the Ministry of Science, Technological Development and Innovation of the Republic of Serbia, grant number 451-03-33/2026–03/200222 and 451-03-33/2026–03/200358. The findings of this study contribute to the achievement of the United Nations 2030 Agenda for Sustainable Development, specifically targeting the second goal, "Zero Hunger." Additionally, authors would like to thank Stefan Simić from Voxellab, Serbia for helpful advice during the realization of experiments.

Supplementary materials

Supplementary material associated with this article can be found, in the online version, at doi:10.1016/j.afres.2026.102013.

Data availability

Data will be made available on request.

References

Agarwal, D., Wallace, A., Kim, E. H. J., Wadamori, Y., Feng, L., Hedderley, D., & Morgenstern, M. P. (2022). Rheological, structural and textural characteristics of 3D-printed and conventionally-produced gluten-free snack made with chickpea and lupin flour. *Future Foods, 5*, Article 100134. https://doi.org/10.1016/j.fufo.2022.100134

Arora, V. K., & Prithviraj, V. (2022). Printability assessment and optimization of process parameters for 3D printing of rice flour and jaggery paste. *Journal of Biosystems Engineering, 47*(2), 248–262. https://doi.org/10.1007/s42853-022-00143-z

Bao, Y., Li, L., Chen, J., Cao, W., Liu, W., Ren, G., Luo, Z., Pan, L., & Duan, X. (2024). Prediction of 3D printability and rheological properties of different pineapple gel formulations based on LF-NMR. *Food Chemistry: X, 24*, Article 101906. https://doi.org/10.1016/j.fochx.2024.101906

Barrios-Rodríguez, Y. F., Igual, M., Martínez-Monzó, J., & García-Segovia, P. (2024). Multivariate evaluation of the printing process on 3D printing of rice protein. *Food Research International, 176*, Article 113838. https://doi.org/10.1016/j.foodres.2024.113838

Baş, D., & Boyacı, İ. H. (2007). Modeling and optimization I: Usability of response surface methodology. *Journal of Food Engineering, 78*(3), 836–845. https://doi.org/10.1016/j.jfoodeng.2005.11.024

Belović, M., Torbica, A., Vujasinović, V., Radivojević, G., Perović, L., & Bokić, J. (2025). Technological properties, shelf life and consumers' acceptance of high-fibre cookies prepared with juice processing by-products. *Food Science and Technology International, 31*(7), 638–648. https://doi.org/10.1177/10820132241240329

Bulut, E. G., & Candoğan, K. (2022). Development and characterization of a 3D printed functional chicken meat based snack: Optimization of process parameters and gelatin level. *LWT, 154*, Article 112768. https://doi.org/10.1016/j.lwt.2021.112768

Carranza, T., Guerrero, P., de la Caba, K., & Etxabide, A. (2023). Texture-modified soy protein foods: 3D printing design and red cabbage effect. *Food Hydrocolloids, 145*, Article 109141. https://doi.org/10.1016/j.foodhyd.2023.109141

Carvajal-Mena, N., Tabilo-Munizaga, G., Saldaña, M. D., Pérez-Won, M., Herrera-Lavados, C., Lemus-Mondaca, R., & Moreno-Osorio, L. (2023). Three-dimensional printing parameter optimization for salmon gelatin gels using artificial neural networks and response surface methodology: Influence on physicochemical and digestibility properties. *Gels, 9*(9), 766. https://doi.org/10.3390/gels9090766

Chelladurai, S. J. S., Murugan, K., Ray, A. P., Upadhyaya, M., Narasimharaj, V., & Gnanasekaran, S. (2021). Optimization of process parameters using response surface methodology: A review. *Materials Today: Proceedings, 37*, 1301–1304. https://doi.org/10.1016/j.matpr.2020.06.466

Cheng, Z., Qiu, Y., Bian, M., He, Y., Xu, S., Li, Y., Ahmad, I., Ding, Y., & Lyu, F. (2024). Effect of insoluble dietary fiber on printing properties and molecular interactions of 3D-printed soy protein isolate-wheat gluten plant-based meats. *International Journal of Biological Macromolecules, 258*, Article 128803. https://doi.org/10.1016/j.ijbiomac.2024.128803

Deng, Y., Cheng, K., Shao, X., Dong, X., Jiang, H., & Xiao, G. (2023). Effects of drying method on the stability and quality of post-processing of 3D-printed processed cheese. *Drying Technology, 41*(6), 1060–1067. https://doi.org/10.1080/07373937.2022.2126494

Derossi, A., Caporizzi, R., Azzollini, D., & Severini, C. (2018). Application of 3D printing for customized food. A case on the development of a fruit-based snack for children. *Journal of Food Engineering, 220*, 65–75. https://doi.org/10.1016/j.jfoodeng.2017.05.015

Derossi, A., Caporizzi, R., Ricci, I., & Severini, C. (2019). Critical variables in 3D food printing. *Fundamentals of 3D food printing and applications* (pp. 41–91). Academic Press. https://doi.org/10.1016/B978-0-12-814564-7.00003-1

Derossi, A., Corradini, M. G., Caporizzi, R., Oral, M. O., & Severini, C. (2023). Accelerating the process development of innovative food products by prototyping through 3D printing technology. *Food Bioscience, 52*, Article 102417. https://doi.org/10.1016/j.fbio.2023.102417

Derossi, A., Paolillo, M., Caporizzi, R., & Severini, C. (2020). Extending the 3D food printing tests at high speed. Material deposition and effect of non-printing movements on the final quality of printed structures. *Journal of Food Engineering, 275*, Article 109865. https://doi.org/10.1016/j.jfoodeng.2019.109865

Derossi, A., Spence, C., Corradini, M. G., Jekle, M., Fahmy, A. R., Caporizzi, R., Devahastin, S., Moses, J. A., Le-Bail, A., Zhou, W., Zhang, M., Bhandari, B., & Severini, C. (2024). Personalized, digitally designed 3D printed food towards the reshaping of food manufacturing and consumption. *npj Science of Food, 8*(1), 54. https://doi.org/10.1038/s41538-024-00296-5

Dordević, D., Těšíková, K., Mikuláškova, H. K., Martinez-Monzo, J., Matas, A., Dordević, S., & Kushkevych, I. (2025). Correction: Development of lentil flour-enriched chocolate matrices for 3D printing: Impact on bioactivity, rheology, and texture. *Food and Bioprocess Technology, 18*(5), 4858. https://doi.org/10.1007/s11947–025–03747–3. -4858.

Equbal, A., Murmu, R., Kumar, V., & Equbal, M. A. (2024). A recent review on advancements in dimensional accuracy in fused deposition modeling (FDM) 3D printing. *AIMS Materials Science, 11*(5), 950–990. https://doi.org/10.3934/matersci.2024046

FAO, F. (2018). *The future of food and agriculture: Alternative pathways to 2050* (p. 228). Rome: Food and Agriculture Organization of the United Nations. https://www.fao.org/3/I8429EN/i8429en.pdf.

Feng, C., Zhang, M., Bhandari, B., & Ye, Y. (2020). Use of potato processing by-product: Effects on the 3D printing characteristics of the yam and the texture of air-fried yam snacks. *LWT, 125*, Article 109265. https://doi.org/10.1016/j.lwt.2020.109265

Guénard-Lampron, V., Liu, X., Masson, M., & Blumenthal, D. (2023). Screening of different flours for 3D food printing: Optimization of thermomechanical process of soy and rye flour dough. *Innovative Food Science & Emerging Technologies, 87*, Article 103394. https://doi.org/10.1016/j.ifset.2023.103394

Guénard-Lampron, V., Masson, M., Leichtnam, O., & Blumenthal, D. (2021). Impact of 3D printing and post-processing parameters on shape, texture and microstructure of carrot appetizer cake. *Innovative Food Science & Emerging Technologies, 72*, Article 102738. https://doi.org/10.1016/j.ifset.2021.102738

Guo, C., Zhang, M., & Bhandari, B. (2019). Model building and slicing in food 3D printing processes: A review. *Comprehensive Reviews in Food Science and Food Safety, 18*(4), 1052–1069. https://doi.org/10.1111/1541-4337.12443

Habuš, M., Benković, M., Iveković, D., Pavičić, T. V., Mustač, N.Č., Voučko, B., Ćurić, D., & Novotni, D. (2022). Effect of oil content and enzymatic treatment on dough rheology and physical properties of 3D-printed cereal snack. *Journal of Cereal Science, 108*, Article 103559. https://doi.org/10.1016/j.jcs.2022.103559

Habuš, M., Golubić, P., Vukušić Pavičić, T., Čukelj Mustač, N., Voučko, B., Herceg, Z., Ćurić, D., & Novotni, D. (2021). Influence of flour type, dough acidity, printing temperature and bran pre-processing on browning and 3D printing performance of snacks. *Food and Bioprocess Technology, 14*(12), 2365–2379. https://doi.org/10.1007/s11947-021-02732-w

Hao, L., Mellor, S., Seaman, O., Henderson, J., Sewell, N., & Sloan, M. (2010). Material characterisation and process development for chocolate additive layer manufacturing. *Virtual and Physical Prototyping, 5*(2), 57–64. https://doi.org/10.1080/17452751003753212

Huang, M. S., Zhang, M., & Bhandari, B. (2019). Assessing the 3D printing precision and texture properties of brown rice induced by infill levels and printing variables. *Food and Bioprocess Technology, 12*(7), 1185–1196. https://doi.org/10.3390/foods12101185

Jiang, H., Zheng, L., Zou, Y., Tong, Z., Han, S., & Wang, S. (2019). 3D food printing: Main components selection by considering rheological properties. *Critical Reviews in Food Science and Nutrition, 59*(14), 2335–2347. https://doi.org/10.1080/10408398.2018.1514363

Jiao, X., Ren, G., Law, C. L., Li, L., Cao, W., Luo, Z., Pan, L., Duan, X., Chen, J., & Liu, W. (2024). Novel strategy for optimizing of corn starch-based ink food 3D printing process: Printability prediction based on BP-ANN model. *International Journal of Biological Macromolecules, 276*, Article 133921. https://doi.org/10.1016/j.ijbiomac.2024.133921

Kadival, A., Kour, M., Meena, D., & Mitra, J. (2023). Extrusion-based 3D food printing: Printability assessment and improvement techniques. *Food and Bioprocess Technology, 16*(5), 987–1008. https://doi.org/10.1007/s11947-022-02931-z

Kewuyemi, Y. O., Kesa, H., Meijboom, R., Alimi, O. A., & Adebo, O. A. (2022). 3D food printing improves color profile and structural properties of the derived novel whole-grain sourdough and malt biscuits. *Scientific Reports, 12*(1), Article 12347. https://doi.org/10.1038/s41598-022-16659-5

Kim, J., Kim, J. S., Lim, J. H., & Moon, K. D. (2024). Effects of isolated pea protein on honeyed red ginseng manufactured by 3D printing for patients with dysphagia. *LWT, 191*, Article 115570. https://doi.org/10.1016/j.lwt.2023.115570

Krishnaraj, P., Anukiruthika, T., Choudhary, P., Moses, J. A., & Anandharamakrishnan, C. (2019). 3D extrusion printing and post-processing of fibre-rich snack from indigenous composite flour. *Food and Bioprocess Technology, 12*(10), 1776–1786. https://doi.org/10.1007/s11947-019-02336-5

Lee, C. P., & Hashimoto, M. (2024). Prediction of textural properties of 3D-printed food using response surface methodology. *Heliyon, 10*(7). https://doi.org/10.1016/j.heliyon.2024.e27658

Liu, L., & Ciftci, O. N. (2021). Effects of high oil compositions and printing parameters on food paste properties and printability in a 3D printing food processing model. *Journal of Food Engineering, 288*, Article 110135. https://doi.org/10.1016/j.jfoodeng.2020.110135

Liu, Z., & Zhang, M. (2021). Texture properties of microwave post-processed 3D printed potato snack with different ingredients and infill structure. *Future Foods, 3*, Article 100017. https://doi.org/10.1016/j.fufo.2021.100017

Liu, Z., Zhang, M., Bhandari, B., & Wang, Y. (2017). 3D printing: Printing precision and application in food sector. *Trends in Food Science and Technology, 69*, 83–94. https://doi.org/10.1016/j.tifs.2017.08.018

Livingstone, D. J. (Ed.). (2008), *Artificial neural networks: Methods and applications: 458*. *Artificial neural networks: Methods and applications* (pp. 185–202). Totowa, NJ, USA: Humana Press. https://doi.org/10.1007/978-1-60327-101-1.

Loskot, J., Jezbera, D., Loskot, R., Bušovský, D., Barylski, A., Glowka, K., Duda, P., Aniolek, K., Voglova, K., & Zubko, M. (2023). Influence of print speed on the microstructure, morphology, and mechanical properties of 3D-printed PETG products. *Polymer Testing, 123*, Article 108055. https://doi.org/10.1016/j.polymertesting.2023.108055

Maldonado-Rosas, R., Tejada-Ortigoza, V., Cuan-Urquizo, E., Mendoza-Cachu, D., Morales-de La Pena, M., Alvarado-Orozco, J. M., & Campanella, O. H. (2022). Evaluation of rheology and printability of 3D printing nutritious food with complex formulations. *Additive Manufacturing, 58*, Article 103030. https://doi.org/10.1016/j.addma.2022.103030

Mallesham, P., Parveen, S., Pandiselvam, R., Rajkumar, P., & Naik, R. (2024). Characterisation of 3D printing cake batter with xanthan gum and optimization of printing parameters using response surface methodology. *International Journal of Gastronomy and Food Science, 38*, Article 101026. https://doi.org/10.1016/j.ijgfs.2024.101026

Moon, J., Gbadago, D. Q., Hwang, G., Lee, D., & Hwang, S. (2022). Software platform for high-fidelity-data-based artificial neural network modeling and process optimization in chemical engineering. *Computers & Chemical Engineering, 158*, Article 107637. https://doi.org/10.1016/j.compchemeng.2021.107637

Montero, C. M., Matas, A., Igual, M., Martínez-Monzó, J., & García-Segovia, P. (2025). Influence of internal printing pattern and infill on morphological and dimensional properties of gluten-free bread manufactured by 3D printing. *Future Foods*. , Article 100715. https://doi.org/10.1016/j.fufo.2025.100715

Mudau, M., & Adebo, O. A. (2024). Three dimensional (3D)-printed foods: A review of recent advances in their ingredients, printing techniques, food printers, post-processing methods, consumer acceptance and safety. *Journal of Food Process Engineering, 47*(5), Article e14621. https://doi.org/10.1111/jfpe.14621

Mustač, N.Č., Pastor, K., Kojić, J., Voučko, B., Ćurić, D., Rocha, J. M., & Novotni, D. (2023). Quality assessment of 3D-printed cereal-based products. *LWT, 184*, Article 115065. https://doi.org/10.1016/j.lwt.2023.115065

Oropallo, W., & Piegl, L. A. (2016). Ten challenges in 3D printing. *Engineering with Computers, 32*(1), 135–148. https://doi.org/10.1007/s00366-015-0407-0

Oyinloye, T. M., & Yoon, W. B. (2021). Application of computational fluid dynamics (CFD) simulation for the effective design of food 3D printing (A review). *Processes, 9*(11), 1867. https://doi.org/10.3390/pr9111867

Pérez, B., Nykvist, H., Brøgger, A., Larsen, M., & Falkeborg, M. (2019). Impact of macronutrients printability and 3D-printer parameters on 3D-food printing: A review. *Food Chemistry, 287*, 249–257. https://doi.org/10.1016/j.foodchem.2019.02.090

Pulatsu, E., Su, J. W., Lin, J., & Lin, M. (2020). Factors affecting 3D printing and post-processing capacity of cookie dough. *Innovative Food Science & Emerging Technologies, 61*, Article 102316. https://doi.org/10.1016/j.ifset.2020.102316

Pradhan, A., Saha, D., & Tripathy, P. P. (2025). A multivariate study on the effect of 3D printing parameters on the printability of gluten-free composite dough. *Journal of the Science of Food and Agriculture, 105*(4), 2578–2593. https://doi.org/10.1002/jsfa.14031

Radoš, K., Pastor, K., Kojić, J., Drakula, S., Dujmić, F., Novotni, D., & Čukelj Mustač, N. (2023a). Influence of infill level and post-processing on physical parameters and betaine content of enriched 3D-printed sweet snacks. *Foods (Basel, Switzerland), 12*(24), 4417. https://doi.org/10.3390/foods12244417

Radoš, K., Benković, M., Mustač, N.Č., Habuš, M., Voučko, B., Pavičić, T. V., Ćurić, D., Ježek, D., & Novotni, D. (2023b). Powder properties, rheology and 3D printing quality of gluten-free blends. *Journal of Food Engineering, 338*, Article 111251. https://doi.org/10.1016/j.jfoodeng.2023.111251

Rogers, H., & Srivastava, M. (2021). Emerging sustainable supply chain models for 3D food printing. *Sustainability, 13*(21), Article 12085. https://doi.org/10.3390/su132112085

Sadaf, M., Cano, S., Gonzalez-Gutierrez, J., Bragaglia, M., Schuschnigg, S., Kukla, C., Holzer, C., Vály, L., Kitzmantel, M., & Nanni, F. (2022). Influence of binder composition and material extrusion (MEX) parameters on the 3D printing of highly filled copper feedstocks. *Polymers, 14*(22), 4962. https://doi.org/10.3390/polym14224962

Severini, C., Derossi, A., & Azzollini, D. (2016). Variables affecting the printability of foods: Preliminary tests on cereal-based products. *Innovative Food Science & Emerging Technologies, 38*, 281–291. https://doi.org/10.1016/j.ifset.2016.10.001

Shi, S., Wen, J., Geng, H., Zhan, X., & Liu, Y. (2024). Physicochemical properties, structural properties and gels 3D printing properties of wheat starch. *International Journal of Biological Macromolecules, 261*, Article 129885. https://doi.org/10.1016/j.ijbiomac.2024.129885

Simeunović, J., Miljanić, J., Kokić, B., Perović, L., Jovančević, J., Glušac, J., & Kojić, J. (2025). Protein fortification of millet-based gluten-free snacks designed for 3D printing. *Foods (Basel, Switzerland), 14*(24), 4308. https://doi.org/10.3390/foods14244308

Sun, J., Peng, Z., Yan, L., Fuh, J. H., & Hong, G. S. (2015). 3D food printing—An innovative way of mass customization in food fabrication. *International Journal of Bioprinting, 1*(1), 27–38. https://doi.org/10.1016/j.promfg.2015.09.057

Thangalakshmi, S., Arora, V. K., Kaur, B. P., Singh, R., Malakar, S., Rathi, S., & Tarafdar, A. (2022). Effect of steaming as postprocessing method on rice flour and jaggery 3D printed construct. *Journal of Food Quality, 2022*(1), Article 3531711. https://doi.org/10.1155/2022/3531711

Tyupova, A., & Harasym, J. (2024). Valorization of fruit and vegetables industry by-streams for 3D printing—A review. *Foods (Basel, Switzerland), 13*(14), 2186. https://doi.org/10.3390/foods13132186

Usman, M., Lu, Y., Jin, Z., Rao, J., & Xu, M. (2025). Germination-driven modifications in pulse carbohydrates for optimized 3D food printing inks and structures. *Food Chemistry*. , Article 147284. https://doi.org/10.2139/ssrn.5294979

Wang, Y., Chen, H., Liu, Q., Zhao, R., Liu, W., Liu, S., Zhang, L., & Hu, H. (2023). An optimized 3D-printed capsule scaffold utilizing artificial neural network for the targeted delivery of chlorogenic acid to the colon. *Food Research International, 174*, Article 113612. https://doi.org/10.1016/j.foodres.2023.113612

Wu, J. (2018). Study on optimization of 3D printing parameters. In *IOP conference series: Materials science and engineering, 392*. IOP Publishing, Article 062050. https://doi.org/10.1088/1757-899X/392/6/062050

Yang, F., Guo, C., Zhang, M., Bhandari, B., & Liu, Y. (2019). Improving 3D printing process of lemon juice gel based on fluid flow numerical simulation. *Lwt, 102*, 89–99. https://doi.org/10.1016/j.lwt.2018.12.031

Zhang, Z., Zhang, C., Fan, Z., Chen, Z., Liu, X., Zhang, G., Wang, S., Shen, Y., Wang, D., Li, W., R, A., & Fan, S. (2024). Development and characterization of whole-grain buckwheat biscuit formula based on extruded 3D printing technology. *Journal of Food Measurement and Characterization, 18*(12), 9766–9780. https://doi.org/10.1007/s11694-024-02914-y